Journal of Power Sources 196 (2011) 3479–3484

Contents lists available at ScienceDirect

Journal of Power Sources

journal homepage: www.elsevier.com/locate/jpowsour

Influence of ageing in fuel cell on membrane/electrodes interfaces

A.S. Danerol[a], C. Bas[a,*], L. Flandin[a], E. Claude[b], N.D. Alberola[a]

[a] Laboratoire Matériaux Organiques à Propriétés Spécifiques (UMR CNRS 5041), Université de Savoie, 73230 Le Bourget du Lac, France
[b] AXANE, 2 rue de Clémencière, BP15, 38360 Sassenage, France

ARTICLE INFO

Article history:
Received 27 May 2010
Received in revised form 3 December 2010
Accepted 11 December 2010
Available online 21 December 2010

Keywords:
PEMFC
Active layers
Membrane
Interface
Degradation
Fuel cells

ABSTRACT

The changes in properties within membrane electrode assemblies (MEAs) aged in a stack functioning at constant-power operation (0.12 W cm^{-2}) for several durations (0, 347, 892, and 1397 h) were characterized. An important effort was placed into better understanding interfaces. Two tests were thus developed to investigate the changes in each active layer/membrane interface. Both techniques demonstrated that the mechanical bounding of both cathode and anode to the polymer membrane improve with the functioning time in fuel cell. This phenomenon was further attributed to Pt dissolution and diffusion/precipitation within the polymer membrane and to a diffusion/crystallization of the binding agent in the vicinity of the electrode/membrane interfaces.

1. Introduction

Proton exchange membrane fuel cells (PEMFCs) are promising power sources since they directly convert chemical into electrical energy with environmental benefits. The key component in a PEMFC is the membrane electrode assembly (MEA) is a multilayer structure constituted by a polymer membrane acting as a solid electrolyte, coated on both sides by active layers, the cathode and the anode. This three-component system is then covered by gas diffusion layers on either side. The active layers are made of porous carbon supported nanometer sized Pt catalyst, bounded together by an oligomeric ionomer similar to the polymer membrane.

It is now well-accepted that the durability of a fuel cell stack are mainly governed by that of the MEA, and more specifically by its active layers. Several origin for the electrode degradation have been pointed out in the literature (i) the decrease in electrochemical activity due to the contamination of the Pt catalyst with either pollutants coming from the input gas [1–5] or CO_2 poisoning caused by the carbon support corrosion [6–11], (ii) catalyst particle dissolution yielding to the coarsening of Pt particles and subsequently a reduction of the specific surface area [12–19] emphasized by a loss in the overall amount of catalyst in the electrode [13,18,20], (iii) carbon corrosion mainly observed at the cathode side attributed to the presence of oxygen which may induce a structural collapse of the electrode [5,8,9,21], (iv) catalyst layer ionomer degradation [22,23]. The relative contributions of these degradation mechanisms strongly depend on the working conditions of the fuel cell [24], namely (i) the number and amplitude of voltage cycles, (ii) the time at high cathode potential, and (iii) changes in relative humidity [18,25,26]. For example, the Pt dissolution/diffusion/aggregation mechanism was revealed prominent at the cathode side under high potential cycling rates [27,28]

Although this parameter has not been studied much in the literature [29], it seems important to quantify the adhesion between active layers and membrane [30]. This interface will for instance be submitted to a shear in service as result in dimensional changes of the membrane, with variations in temperature, and relative humidity. The study of the active layer to membrane interface may also be relevant to understand changes in either component as well as the undesirable evolution of the electrical properties.

2. Experimental

2.1. Materials

As-received and aged commercial MEAs were provided by Axane Company. The MEAs are multilayer structures based on perfluorosulfonic acid polymer membrane (Nafion®), coated on both sides by active layers covered by gas diffusion layers (carbon cloths). Electrode layers are constituted by porous carbon supported nanosized Pt catalyst, with an ionomer binding agent which chemical nature was similar to that of the membrane [28]. The active layers initially contained 40 ± 1 and 28 ± 2 wt.% of carbon and platinum, respectively. The platinum electroactive area was close to

* Corresponding author. Tel.: +33 4 79 75 86 24; fax: +33 4 79 75 86 15.
E-mail address: cobas@univ-savoie.fr (C. Bas).

0378-7753/$ – see front matter © 2010 Elsevier B.V. All rights reserved.
doi:10.1016/j.jpowsour.2010.12.014

0.0035 cm^2 [31]. The amount of binding agent was close to 30 wt.% in as-received electrodes. The MEAs were industrially processed through the carbon coated membrane (CCM) process. As-received MEAs were never mounted in a stack and thus never submitted to mechanical stresses upon assembling. Aged MEAs were utilized in a 55 cells stack system in a constant power mode (0.12 W cm^{-2}) for several durations: 347, 892 and 1397 h. The current density was ~0.18 A cm^{-2} corresponding to a cathode potential close to 0.67 V with respect to the reversible hydrogen potential (RHE). The cathode was fed with humidified air (75% relative humidity (RH) at atmospheric pressure) and the anode with dry pure hydrogen (with a controlled overpressure of 0.2 bars). The gas flow rates were 5 and 30 NL min^{-1} for H_2 and air, respectively. The aged MEAs were sampled from intermediates regions of the stack where the temperature is almost constant, close to 60 °C. At least three different specimens for each ageing time were systematically investigated. The characterizations focused on three-layer systems, namely the membrane and the two active layers. The gas diffusion layers were thus gently removed from MEAs prior to measurements, without damaging the electrodes, thanks to the low adhesion to carbon cloths resulting from CCM process.

In addition, for characterizations of the sole membrane, uncoated samples were obtained by immersion in a 50/50 vol./vol.% water/ethanol mixture in an ultrasonic bath until a clear membrane was obtained, which took up to 4 h (see below).

2.2. Microscopy investigations

Morphology analyses were performed with a scanning electron microscope (SEM – Leica Stereoscan 440 microscope) at 20 kV accelerating voltage in the electron backscattered mode. Energy dispersive X-ray (EDX) analyses (silicon drift detector) were also carried out to locate the platinum. The electrode coated membranes were first cut at room temperature into small pieces using ceramic scissors. Then, these small slices were epoxy-embedded at room temperature and sample cross sections were carefully polished and metalized.

The distribution in size of the catalyst particle was measured from transmission electron microscopy images (TEM-Philips CM120 microscope at 120 kV) performed on cross-sectional thin slices obtained by cryogenic ultramicryotomy. The quantitative image analysis were then performed on segmented images with ImageJ software [32].

2.3. X-ray diffraction (XRD) analyses

XRD diffractograms were obtained at ambient temperature on a Bruker D8 Advance X-ray diffractometer, using Cu Kα radiation (λ = 1.5418 Å). Samples were rotationally analyzed and the diffraction scans were collected over a period of about 20 min from 4° to 90° (2θ) using a scan increment of 0.02°.

XRD analyses were carried out on as-received and aged samples, both anode and cathode sides were systematically analyzed. Diffractograms were taken with and without active layers.

2.4. Thermogravimetry analysis

The active layers detached from MEAs (by immersion in a water/ethanol with ultrasonic both), were characterized after filtration, by thermogravimetry analysis (TGA TA 2050) under helium gas flow, at the usual heating rate of 10 °C min^{-1}. This technique was utilized to characterize the three component of the active layer, namely the carbon support, the Pt catalyst, and the ionomer binding agent.

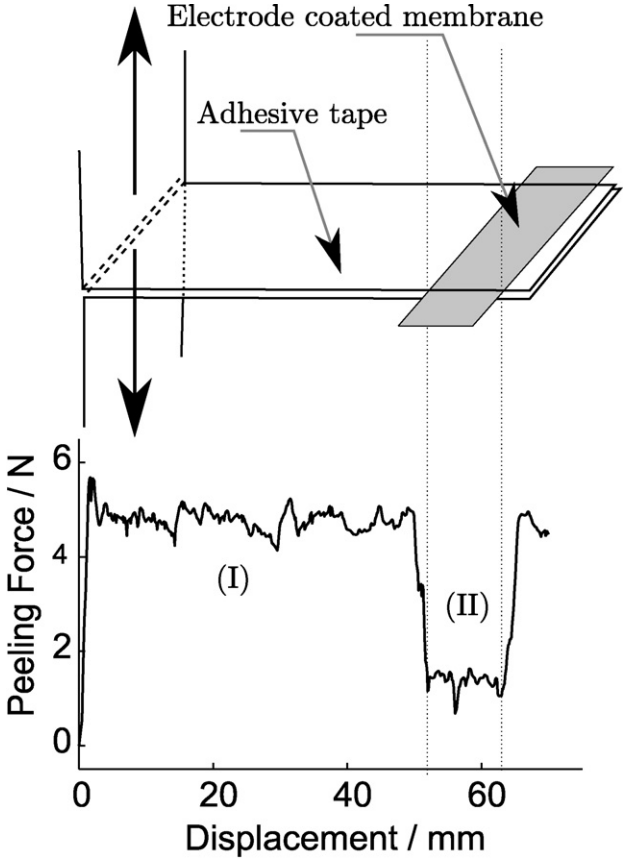

Fig. 1. Scheme of the mechanical *T*-peel test (top) peeling test curve recorded for a 347 h aged sample (bottom).

2.5. Active layers/membrane interface

Two complementary techniques were utilized to characterize the active layer to membrane interface, (i) sample immersion in a water/ethanol mixture in an ultrasonic bath and (ii) the so-called mechanical *T*-peel test.

2.5.1. Immersion in water/ethanol

Small pieces (1.5 cm × 1.5 cm) of electrode coated membranes were immersed at ambient temperature in a 50/50 vol/vol.% water/ethanol mixture, and kept in an ultrasonic bath. A sample was removed every minute and observed with an optical microscope (Leica) in a transmission mode. The relative surface area with and without electrodes residues could thereby be determined, through basic image analysis, as a function of immersion time.

2.5.2. Mechanical T-peel tests

Pieces of MEAs were sandwiched between a folded adhesive tape (Scotch® Magic™ Tape, 3M). The dimensions of analyzed MEA samples were of about 25 mm in length and 10 mm in width. The tensile tests were performed using an Adamel Lhomargy machine at a constant rate (10 mm min^{-1}), at ambient temperature (23 °C ± 1 °C), and under controlled humidity (50–60% RH). Five samples were systematically tested. Fig. 1 shows an example of raw experimental results (peeling force *vs.* the displacement). In the first part of the curve (I), the strong adhesion of the tape to itself was disregarded; and the actual adhesion between active layer and membrane is measured in part II, after the peeling force dropped and reached a plateau corresponding to the sample.

After peeling, optical microscopy observations of the adhesive tapes (Leica microscope) coupled with image analyses [32] were

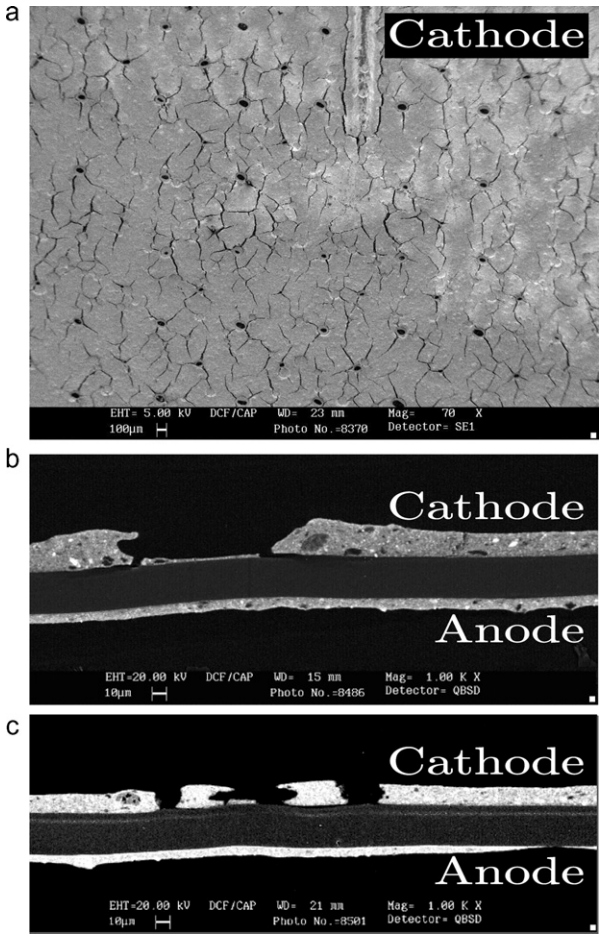

Fig. 2. SEM micrographs of the MEAs: as-received sample cathode flat view (a), and cross sections (b) cross section of a sample aged 1397 (c).

performed to quantify the surface area occupied on the by electrode fragments left on the tape.

3. Results and discussion

Fig. 2 shows SEM pictures of the cathode surface for the as-received sample (a), and the cross sections of as-received (b) and 1397 h aged (c) specimens. For both as-received and aged electrode coated membranes, SEM observations give evidence for holes and cracks within the electrode. These features may originate from the sample preparation procedure, *i.e.*, cutting, epoxy-embedding, and polishing. Nevertheless, the sample without preparation (Fig. 2a), also showed regularly arranged holes, likely to be related to the MEA fabrication. In the initial state, decohesion between membrane and electrode layers were mainly located in the vicinity of these native defects (Fig. 2c).

The thicknesses of both electrodes and membrane were measured on 10 SEM micrographs. A thinning of the electrodes is systematically observed with time, especially for the cathode side. This was already reported and attributed to carbon support corrosion during fuel cell operation [7,33]. The electrode degradation is also accompanied by a decrease in the membrane thickness from 33 to 28 µm, also reported by other [16,29,34] and discussed in detail another paper [35]. SEM observations with EDX analyses revealed, at 892 h or more in service the presence of a "Pt band" within the membrane at about 4–8 µm from the cathode (Fig. 2c), as already described in the literature [12,15,28,31,36]. Interestingly, the Pt band was not detected in front of native defects were no electrochemical activity occurred. This was viewed as confirmation that Pt particles within polymer originated from the cathode during fuel cell operation.

Table 1
Average platinum particle size for as-received and aged samples, derived from XRD and TEM analyses.

Samples		Average particle size (nm)			
		Anode		Cathode	
		XRD ± 0.2	TEM ± 0.3	XRD ± 0.2	TEM ± 0.3
As-received (0 h)		3.7	2.8	3.8	2.9
Aged samples	347 h	3.9	3.9	4.0	3.8
	892 h	5.9	5.3	5.5	5.9
	1397 h	4.6	5.2	4.8	5.4

The average Pt particle sizes within the two active layers were derived from TEM and XRD analyses, and gathered in Table 1. No significant difference in particle size between anode and cathode was detected for a given ageing time. A significant increase in particle size with time was, however, evidenced within the two active layers. This Pt coarsening is detrimental to the specific surface area of the catalyst and thereby to the overall performances of the fuel cell. Pt coarsening has already been observed on the cathode aged MEAs [1,12–14]. The present work confirms that the same phenomenon also exist on the anode side [22]. Different mechanisms were proposed to explain this phenomenon [37]. The decrease in thickness of the two active layers measured in the current work (and the corresponding volume changes), indicates that the purely geometrical contribution might have been overlooked.

Fig. 3 shows TEM micrograph of the 1397 h aged polymer membrane. With increasing the distance to the cathode, Pt particles within the membrane showed changes in size and shape. To illustrate this, Fig. 4 represents the number of particle per unit surface area and the surface distributions *vs.* the distance to cathode. The number of particles was found to progressively decrease, while the particle surface exhibited a maximum at about 5 µm of the cathode. These quantitative measurements were consistent with the qualitative observations with the SEM. The main mechanism to explain the presence of Pt within the solid electrolyte is based on the migration of Pt^{z+}, mainly Pt^{2+}, resulting from the dissolution of Pt favored by load cycling, high potential, and high oxygen partial pressure at the cathode [12,21,38,39]. Then, two phenomena may occur: (i) growth of Pt particles on the carbon support, mainly within the

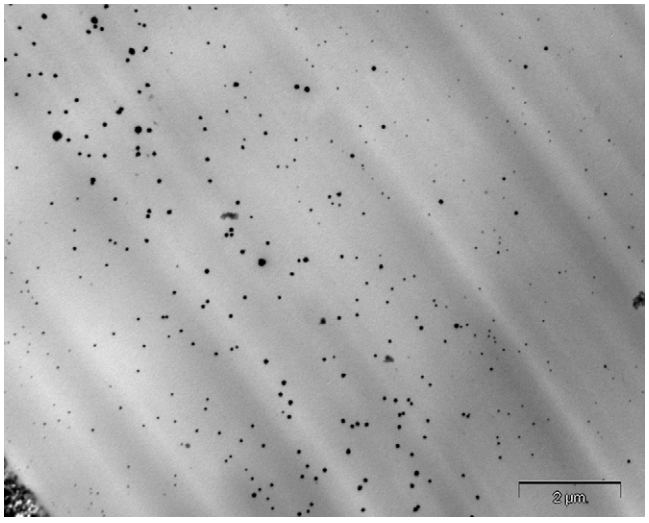

Fig. 3. TEM images of platinum front within the membrane for the sample aged 1397 h.

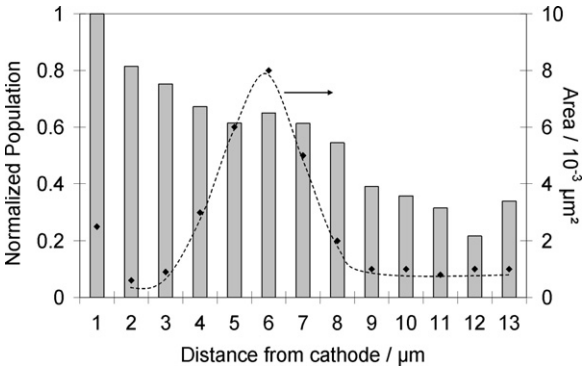

Fig. 4. Distributions of number of particle and surface area within the membrane as a function of the distance to cathode (1397 h sample).

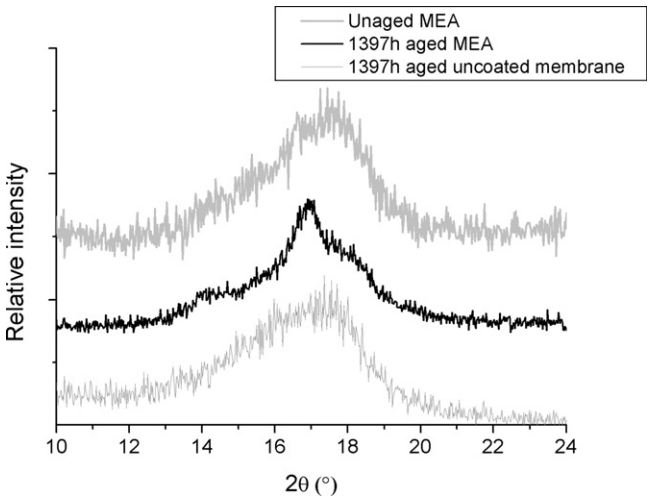

Fig. 5. XRD diffractograms of as-received sample, 1397 h aged electrode coated membrane and 1397 h aged after removing electrodes.

cathode, and (ii) Pt^{z+} diffusion in the membrane and reduction by the hydrogen gas cross-over.

These mechanisms do not account for the plausible role played by the binding agent. This interface coupling agent contributes not only to the proton conduction, but also to both the internal electrode cohesion, and its adhesion to the polymer membrane. In order to get insights on the plausible role played by the binding agent, XRD characterizations were performed to investigate the modifications of the electrode on ageing. For the as-received and the longest aged electrode coated membranes, diffractograms were recorded (Fig. 5) from 10° to 30° 2θ range, where the XRD polymer profile is expected [40,41]. The diffractogram obtained for the longest aged MEA after removing the electrodes was also plotted. The as-received MEA exhibited a broad 2θ peak ranging from 13° to 20°. This diffractogram resulted from the superimposed profiles of the polymer electrolyte and the ionomer agent that initially presented similar chemical structures. This XRD pattern in Fig. 5 is characteristic of perfluorinated sulfonatic acid polymer resulting from the convolution of amorphous and crystalline scattering of the polyfluorocarbon chains of, respectively, at 16° and 17.5° [40,41]. The ageing induced two main changes in the XRD diffractograms, (i) a new sharp peak at about 17.5°, and (ii) two shoulder-peaks on either side of the main peak, at 14° and 18°. Because these two features were essentially absent from the aged MEA after removing the electrode, it was concluded that a textured phase developed within the active layers. The organization of the carbon support within the electrodes would, however, be detected in the 26° range [42,43]. It thus seemed reasonable to attribute new peaks to the binding agent. In addition, crystalline PTFE present a diffraction peak at 18°, corresponding to the (1 1 0) planes [43,44]. It was therefore hypothesized that the binding agent underwent a chemical degradation of its lateral groups, promoting its organization. It seemed necessary to study the consequences on the membrane/active layer interface.

To qualify the active layer/membrane interface, two experimental methods have been developed. The first one results from OM observations in transmission mode after various time of solvent treatments. Because a single carbon layer is efficient enough to stop the photon beam, this technique was found essentially sensitive to the mechanically strongest active layer. A representative matrix of micrographs with different ageing and immersion times is presented in Fig. 6.

The influence of the MEA ageing is really striking. This series of pictures clearly demonstrated the increase in interfacial strength with time in service, as shown by the amount of electrode fragments remaining on the membrane that monotonously increased with time in service for a given immersion time (Fig. 6).

For the shortest immersion time, the new MEA still exhibited few electrode fragments, but after 3 min in the ultrasonic bath both active layers were fully removed. It was further evidenced with SEM cross-views that the cathode was actually entirely detached after less than a minute and that only part of the anode remained. Although delayed in immersion time, the same observation was made for the all the specimen, namely the cathode is first remove and then the anode. An example is provided for the longest duration in service (1397 h), after 4 min immersion time (Fig. 7). On this picture the cathode was almost entirely detached, whereas the anode still remained almost free of degradation. As described in Section 2, for all specimens both active layers could eventually be removed

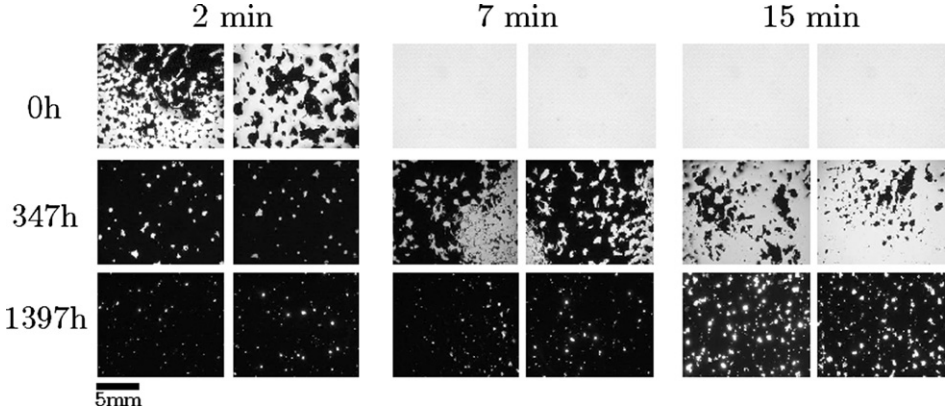

Fig. 6. Optical micrographs in a transmission mode of as-received and aged MEAs for different immersion times.

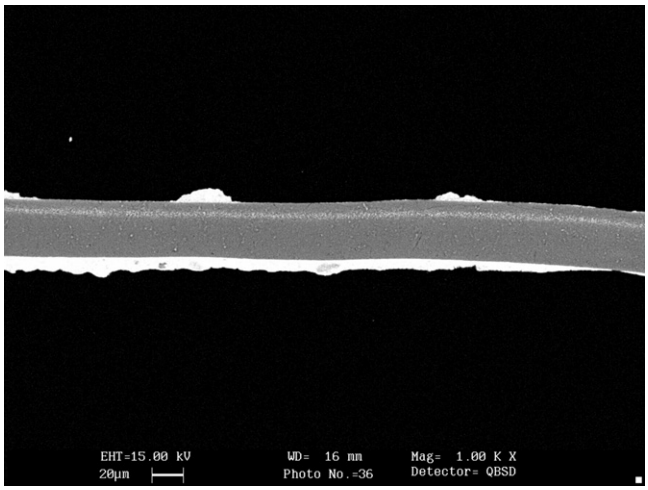

Fig. 7. SEM micrographs of 1397 h aged MEA after 4 min immersion time in water/ethanol mixture.

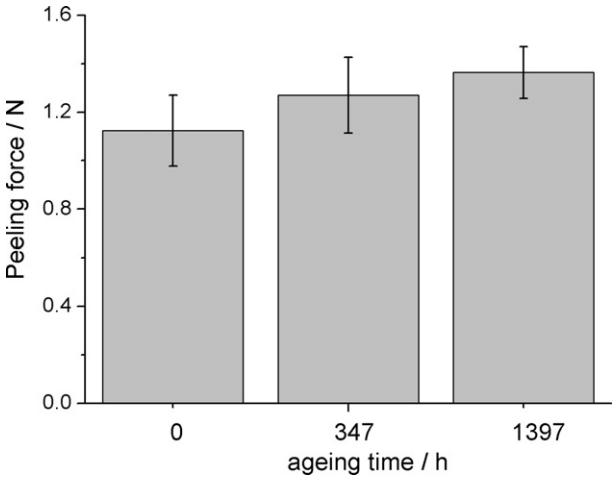

Fig. 9. Peeling forces for as-received and aged electrode coated membranes, *T*-peel tests.

after a long time in the ultrasonic bath, even if the process could take up to 4 h.

A quantitative image analysis was performed on the pictures in Fig. 6. The remaining anode surface fraction was plotted in Fig. 8 for the different samples as a function of the immersion time. On this graph, the as-received sample obviously confirmed that both active layers were easily detached after very few minutes in the ultrasonic bath. More interestingly, the longest aged sample exhibited no significant change on the quantitative point of view. In other words, the white spots that look obvious in Fig. 6 (1397 h, 15 min) only represented low fractions of the images. Since the cathode layer was entirely removed for these immersion times (Fig. 7), the remaining fragments solely corresponded to the anode which was thus strongly bounded to the membrane. A closer look at the intermediate ageing time (347 h) demonstrated a progressive decrease in the remaining fragments with ageing time at a given immersion time.

The second test to characterize the active layer/membrane interface was mechanical *T*-peel tests detailed in Fig. 1. It was first noticed that this apparently very symmetrical technique solely measured the adhesion of the cathode which, again, always appeared weaker than the anode. This may be the consequence of the native defects that reduces the adhesion on the cathode side (Fig. 2a), or the result of the differences in thicknesses between anode and cathode.

Fig. 9 presents the peeling force required to peel the cathode fragments from the membrane. A significant monotonous increase was evidenced, which seemed to indicate that, as far as mechanical properties are concerned, the cathode/membrane interface also improved with time in service. To better understand this result, the fracture mechanisms were investigated. Therefore, OM observations of adhesive tape were carried out, because it represents a fingerprint of the active layer that was removed from the membrane.

The resulting images are presented in Fig. 10. On these images three distinct levels of gray could noticeably be defined:

- First, the 'white' areas were straightforwardly related to initial native defects because they were uncovered with carbon, and because of the regular pattern they formed with one another.
- Second, the 'black' zones corresponded, on the contrary, to the thickest fragments. The possible loss of adhesion between membrane and active layer evidenced by SEM, gave a persuasive argument that these zones corresponded to a total decohesion between membrane and cathode. These zones were thus attributed to an adhesive fracture mode, at the cathode/membrane interface.
- Third and last, the 'gray' regions were ascribed to cohesive rupture, were the fracture actually occurred within the active layer,

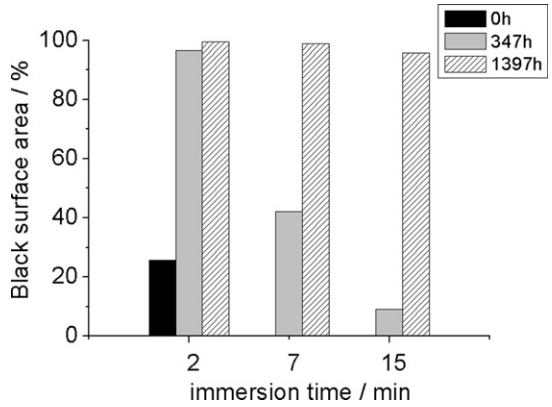

Fig. 8. Relative surface areas of active layers fragments remaining on the membrane *vs.* immersion time for the as-received and aged samples.

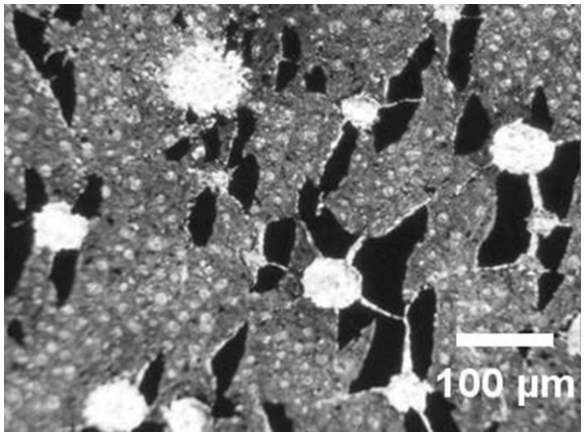

Fig. 10. Optical microscope observations of the adhesive tape after *T*-peel tests performed on as-received sample.

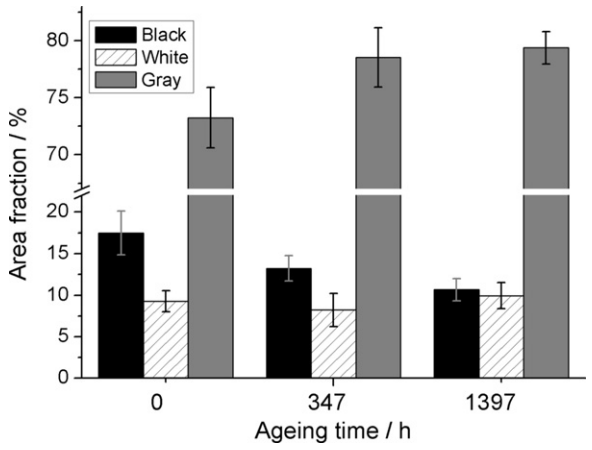

Fig. 11. Relative surface area related to the 'black', 'white' and to the 'gray' regions, for the as-received and aged MEAs.

resulting in an intermediate level of gray. Interestingly, the gray level looked very regular, meaning that the fracture mainly occurred at the given distance inside the cathode.

As a result, the 'black' and 'gray' regions could be used, beside the adhesive strength, to probe the adhesion of the cathode to the membrane. Fig. 11 presents the experimental results obtained with at least ten optical micrographs per ageing time.

First, the 'white' surface area, representing carbon free regions remained basically unchanged with ageing time; this further confirmed their attribution to the native defects. With increasing ageing time, the surface fraction of 'black' area, representing adhesive failure, tend to slightly decrease. Accordingly, the relative amount of 'gray' attributed cohesive rupture increased with time. This result confirmed the mechanical improvement of the cathode to membrane interface with time.

4. Conclusions

This work focused on changes in properties of commercial MEAs aged in a stack functioning at steady state current for several durations (0, 347, and 1397 h). The membrane exhibits a stronger adhesion to the anode than to the cathode, most likely because of the presence of native defects but also because of their differences in thickness. Moreover, in contrast to the literature observations after cycling operations [37], both active layers exhibited an improvement of their mechanical adhesion to the membrane with time in service. This was revealed by the immersion test for the anode/membrane interface and confirmed with the more conventional *T*-peel test for the cathode/membrane interface, although based on very dissimilar mechanisms. For the cathode side, coarsening of Pt particles within the electrodes and development of a Pt band were detected within the membrane in agreement with the literature. These features may originate from Pt dissolution diffusion/precipitation mechanism. In addition, the development of an organized phase within the active layers shown by XRD was detected. The binding agent underwent a chemical degradation of the catalyst layer ionomer as demonstrated by Zhang et al. [23], especially of the lateral groups, leading to a more simple chemical structure, more likely to crystallize. This diffusion/crystallization of the binding agent could also contribute to mechanical improvement of the interfaces.

Acknowledgements

The authors thank the Rhône-Alpes region for doctoral fellowship (A.-S. Danerol) and PAN-H project for financial support.

References

[1] S.Y. Ahn, S.J. Shin, H.Y. Ha, S.A. Hong, Y.C. Lee, T.W. Lim, I.H. Oh, J. Power Sources 106 (2002) 295–303.
[2] J.J. Baschuk, X. Li, Int. J. Energ. Res. 25 (2001) 695–713.
[3] M. Schulze, T. Knori, A. Schneider, A. Gulzow, J. Power Sources 127 (2004) 222–229.
[4] P. Yu, M. Pemberton, P. Plasse, J. Power Sources 144 (2005) 11–20.
[5] X. Yu, S. Ye, J. Power Sources 172 (2007) 145–154.
[6] E. Endoh, S. Terazono, H. Widjaja, Y. Takimoto, Electrochem. Solid-State Lett. 7 (2004) A209–A211.
[7] S.D. Knights, K.M. Colbow, J. St-Pierre, D.P. Wilkinson, J. Power Sources 127 (2004) 127–134.
[8] S. Maass, F. Finsterwalder, G. Frank, R. Hartmann, C. Merten, J. Power Sources 176 (2008) 444–451.
[9] D.A. Stevens, J.R. Dahn, Carbon 43 (2005) 179–188.
[10] W.R. Baumgartner, E. Wallnöfer, T. Schaffer, V. Hacker, P. Peinecke, P. Prenninger, ECS Trans. 3 (2006) 811.
[11] A.A. Franco, M. Gerard, J. Electrochem. Soc. 155 (2008) B367.
[12] P.J. Ferreira, G.J. la, O.Y. Shao-Horn, D. Morgan, R. Makharia, S. Kocha, H.A. Gasteiger, J. Electrochem. Soc. 152 (2005) A2256–A2271.
[13] R.L. Borup, J.R. Davey, F.H. Garzon, D.L. Wood, M.A. Inbody, J. Power Sources 163 (2006) 76–81.
[14] S. Escribano, R. Jamard, A. Morin, S. Solan, L. Guetaz, in: W.H.E. Conference (Ed.), 16th World Hydrogen Energy Conference (WHEC), Lyon, France, 2006.
[15] S. Motupally, in: F.C. Hydrogen, and Infrastructure Technologies (Ed.), UTC Fuel Cells, FY 2003 Progress Report, UTC Fuel Cells, 2003, p. 7.
[16] S.J.C. Cleghorn, D.K. Mayfield, D.A. Moore, J.C. Moore, G. Rusch, T.W. Sherman, N.T. Sisofo, U. Beuscher, J. Power Sources 158 (2006) 446–454.
[17] M. Schulze, A. Schneider, E. Gulzow, J. Power Sources 127 (2004) 213–221.
[18] A. Taniguchi, T. Akita, K. Yasuda, Y. Miyazaki, J. Power Sources 130 (2004) 42–49.
[19] M.S. Wilson, F.H. Garzon, K.E. Sickafus, S. Gottesfeld, J. Electrochem. Soc. 140 (1993) 2872–2877.
[20] A.A. Franco, M. Tembely, J. Electrochem. Soc. 154 (2007) B712–B723.
[21] T. Yoda, H. Uchida, M. Watanabe, Electrochim. Acta 52 (2007) 5997–6005.
[22] J. Xie, D.L. Wood, K.L. More, P. Atanassov, R.L. Borup, J. Electrochem. Soc. 152 (2005) A1011–A1020.
[23] F.-Y. Zhang, S.G. Advani, A.K. Prasad, M.E. Boggs, S.P. Sullivan, T.P. Beebe Jr., Electrochim. Acta 54 (2009) 4025–4030.
[24] S. Zhang, X. Yuan, H. Wang, W. Mérida, H. Zhu, J. Shen, S. Wu, J. Zhang, Int. J. Hydrogen Energy 34 (2009) 388–404.
[25] T. Akita, A. Taniguchi, J. Maekawa, Z. Siroma, K. Tanaka, M. Kohyama, K. Yasuda, J. Power Sources 159 (2006) 461–467.
[26] X. Cheng, C. Peng, M. You, L. Liu, Y. Zhang, Q. Fan, Electrochim. Acta 51 (2006) 4620–4625.
[27] C. He, S. Desai, G. Brown, S. Bollepalli, Electrochem. Soc. Interface 14 (2005) 41–44.
[28] E. Guilminot, A. Corcella, M. Chatenet, F. Maillard, F. Charlot, G. Berthome, C. Iojoiu, J.Y. Sanchez, E. Rossinot, E. Claude, J. Electrochem. Soc. 154 (2007) B1106–B1114.
[29] S.Y. Lee, E.A. Cho, J.H. Lee, H.J. Kim, T.H. Lim, I.H. Oh, J. Won, J. Electrochem. Soc. 154 (2007) 194–200.
[30] S. Kundu, M.W. Fowler, L.C. Simon, S. Grot, J. Power Sources 157 (2006) 650–656.
[31] E. Guilminot, A. Corcella, F. Charlot, F. Maillard, M. Chatenet, J. Electrochem. Soc. 154 (2007) B96–B105.
[32] W. Rasband, in: U.S.N.I.o. Health (Ed.), Bethesda, MA, USA, 1997–2009.
[33] E. Endoh, in: F.C. Seminar (Ed.), Fuel Cell Seminar, San Antonio, TX, 2007.
[34] J. Healy, C. Hayden, T. Xie, K. Olson, R. Waldo, M. Brundage, H. Gasteiger, J. Abbott, Fuel Cells 5 (2005) 302–308.
[35] C. Bas, L. Flandin, A.S. Danerol, E. Claude, E. Rossinot, N.D. Alberola, J. Appl. Polym. Sci. 117 (2010) 2121–2132.
[36] S. Takaichi, H. Uchida, M. Watanabe, Electrochem. Commun. 9 (2007) 1975–1979.
[37] S. Zhang, X.-Z. Yuan, J.N.C. Hin, H. Wang, K.A. Friedrich, M. Schulze, J. Power Sources 194 (2009) 588–600.
[38] R.M. Darling, J.P. Meyers, J. Electrochem. Soc. 150 (2003) A1523–A1527.
[39] L. Kim, C.G. Chung, Y.W. Sung, J.S. Chung, J. Power Sources 183 (2008) 524–532.
[40] P.L. Antonucci, A.S. Aricò, P. Cretì, E. Ramunni, V. Antonucci, Solid State Ionics 125 (1999) 431–437.
[41] T. Hashimoto, M. Fujimura, H. Kawai, in: A. Eisenberg, E.B. Yeager (Eds.) Perfluorinated Ionomer Membranes, ACS Symposium, Washington, DC, 1983, pp. 217–248.
[42] C. Huang, K. Seng Tan, J. Lin, K. Lee Tan, Chem. Phys. Lett. 371 (2003) 80–85.
[43] JCPDS, JCPDS – International Center for Diffraction Data, PA, USA, 1996.
[44] C. Lei, X. Wang, Q. Fang, Y. Gao, D. Tu, Q. Du, Eur. Polym. J. 43 (2007) 4523–4529.